Supporting Information for:

Can CF_3-functionalized La@C_{60} be isolated experimentally and become superconducting?

Jie Guan and David Tománek*

Physics and Astronomy Department, Michigan State University, East Lansing, Michigan 48824, USA

E-mail: tomanek@pa.msu.edu

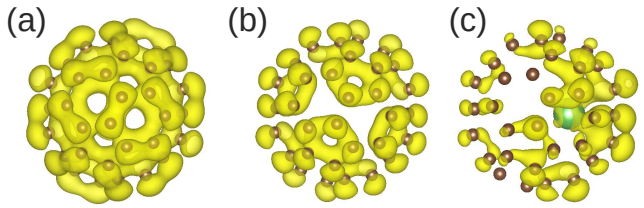

Figure S1: Partial charge distribution ρ_{vc} of (a) the threefold degenerate t_{1u} LUMO of C_{60}, (b) the fivefold degenerate h_u HOMO of C_{60}, and (c) the partly occupied doubly degenerate state of La@C_{60} at the Fermi level. The isosurface value of ρ_{vc} plotted is 0.003 e/Å^3.

Origin of superconductivity in alkali-based M_3C_{60} solids

After a long scientific discussion following the observation of superconductivity in K_3C_{60} and other alkali-based M_3C_{60} intercalation compounds, the following interpretation of this phenomenon has emerged and is now accepted by the scientific community. (i) Alkali-based M_3C_{60} solids are superconductors described well by the BCS theory. The electron-phonon coupling results from a dynamical Jahn-Teller effect on individual C_{60} cages, made possible by retardation, and is confirmed by the isotope effect observed when substituting pure $^{12}C_{60}$ by pure $^{13}C_{60}$ fullerenes. (ii) The dominating role of the intercalated alkali atoms is to partly fill the t_{1u} LUMO of C_{60} that broadens to a narrow band in the M_3C_{60} molecular solid. (iii) Changes in T_c are well described by the changing electron-phonon coupling constant $\lambda = VN(E_F)$ in the McMillan equation. Since the on-ball Bardeen-Pines interaction V does not change, λ is proportional to the electronic density of states at the Fermi level $N(E_F)$, which is roughly inversely proportional to the width of the t_{1u}-derived band. Substituting intercalated K atoms by heavier alkali atoms M leads to an increase of the C_{60}−C_{60} separation, thus reducing the width of the t_{1u} band and consequently increasing the electron-phonon coupling constant λ. We should note that the range of lattice constants allowing superconductivity is limited. Changing the lattice constant changes the inter-ball hopping integral t, while not affecting the on-ball Coulomb integral U. The U/t ratio increases with increasing lattice constant and, beyond a critical value, changes doped C_{60} from a metal to a Mott-Hubbard insulator [1,2].

Frontier states in C_{60} and La@C_{60} molecules

To better understand the effect of the encapsuled La atom on the electronic structure of the La@C_{60} molecule, we calculated the partial charge density of the LUMO and the HOMO of C_{60} as well as that of the doubly degenerate

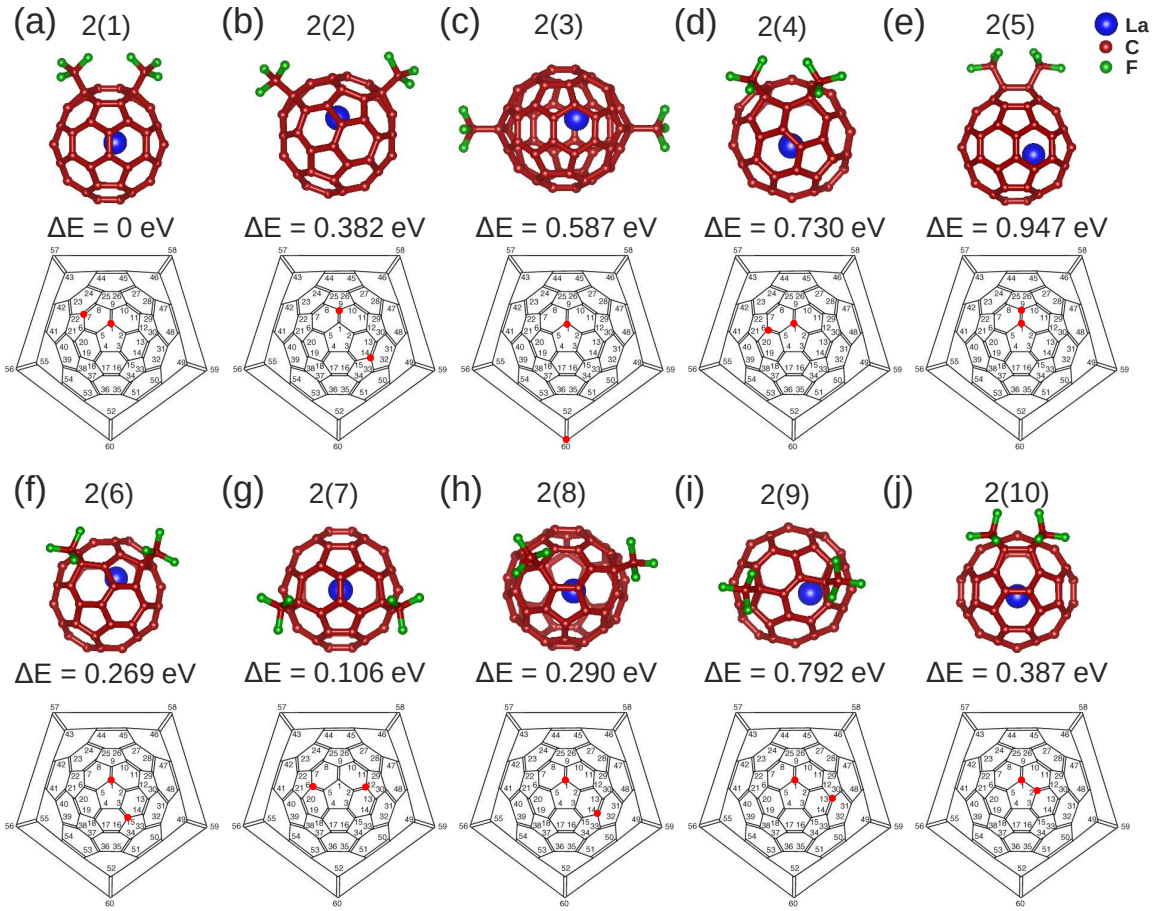

Figure S2: Ten different La@$C_{60}(CF_3)_2$ isomers functionalized with 2 CF_3 radicals. The subfigures display the following isomers: (a) 2(1), (b) 2(2), (c) 2(3), (d) 2(4), (e) 2(5), (f) 2(6), (g) 2(7), (h) 2(8), (i) 2(9), (j) 2(10). The top panels show the ball-and-stick models of the structures, followed by the DFT-PBE relative total energy values ΔE with respect to the most stable isomer. The bottom panels show the Schlegel diagrams of functionalized C_{60} molecules, with the trifluoromethyl sites indicated by the red dots.

level of La@C_{60} at the Fermi level. The corresponding results are presented in Figure S1. As mentioned in the main manuscript, there is an ≈1.6 eV wide gap between the threefold degenerate t_{1u} LUMO and the fivefold degenerate h_u HOMO of the pristine C_{60} molecule. In La@C_{60}, on the other hand, the partly occupied, doubly degenerate state at E_F, which originally belonged to the threefold degenerate LUMO of C_{60}, defines the Fermi level and provides this molecule with a "metallic" character.

The partial charge densities of the LUMO state in Figure S1(a) and the HOMO of C_{60} in Figure S1(b) show that both states are mainly associated with the $p_\perp$ orbitals of C atoms and are equally distributed across all atoms of the pristine fullerene molecule. The partial charge density of the partly occupied state at the Fermi level of the endohedrally doped La@C_{60} molecule, shown in Figure S1(c), resembles that of the t_{1u} LUMO of C_{60}. It consists mostly of $p_\perp$ orbitals of C atoms, with only a small contribution from the enclosed La atom, consistent with our claim that the main role of La is to transfer extra electrons to the π electron network on the C_{60} cage. We note that the charge in the HOMO/LUMO level of La@C_{60} is not distributed evenly across the C_{60} cage. This finding agrees with our Bader charge analysis and is particularly noticeable in Figure S1(c). It can be explained by the positively charged La atom gaining energetically from an off-center displacement, caused by the image-charge interaction, which skews the electron distribution

on the cage towards the encapsulated La atom. Very similar changes occur in the t_{1u}-derived state of C_{60} that acquires a net charge from nearby *exohedral* alkali atoms M in the superconducting M_3C_{60} solid.

Equilibrium structure and stability of different $La@C_{60}(CF_3)_m$ isomers

As mentioned in the main manuscript, the endohedral fullerene $La@C_{60}$ can be functionalized by CF_3 radicals that attach on-top of C atoms and can be arranged in different ways across the C_{60} cage. To identify the most stable $La@C_{60}(CF_3)_m$ geometry, we compared the total energies of different regioisomers containing m trifluoromethyl radicals. Our results for $m = 2, 3, 4$ and 5 are shown in Figures S2, S3, S4 and S5, respectively. Each isomer is identified as $m(i)$, where m denotes the number of CF_3 radicals and i is the assigned isomer number.

Our results for 10 different arrangement of $m = 2$ CF_3 radicals adsorbed on the C_{60} cage are shown in Figure S2. For each regioisomer, we display the optimum geometry, the corresponding Schlegel diagram and relative energy with respect to the most stable isomer $i = 1$. Our results indicate that CF_3 radicals in the most stable $m = 2$ regioisomer are in the para (third neighbor) positions on a single hexagon on the C_{60} surface and the molecule has a C_{2v} symmetry. Other arrangements penalized energetically up to $\lesssim$1 eV, with the least stable arrangement containing CF_3 radicals in adjacent sites. Comparing the relative energies, we found that CF_3 radicals prefer to be close, but not too close on the C_{60} surface.

As seen in Figure S3, a very similar picture emerges for $m = 3$ CF_3 radicals adsorbed on $La@C_{60}$. Comparing the structure of six different isomers in ball-and-stick models as well as Schlegel diagrams, we found that the most stable isomer, shown in Figure S3(a), contains all CF_3 radicals in para (third neighbor) positions on adjacent hexagonal rings on the C_{60} surface, resulting in a mirror symmetry. The second most stable isomer, shown in Figure S3(f), contains CF_3 radicals separated by 5 neighbor distances, is only $\approx$0.1 eV less stable and has a C_3 symmetry. Even though nearest-neighbor arrangements of CF_3 radicals were not considered, other structural candidates incurred an energy penalty of up to $\lesssim$1.3 eV with respect to the most stable isomer.

The structural paradigm changes for $m = 4$ CF_3 radicals adsorbed on the $La@C_{60}$ metallofullerene. Among the 10 regioisomers displayed in Figure S4, the most stable structure, shown in Figure S4(a), contains two pairs of CF_3 radicals in para-arrangement on hexagonal rings that are separated by half the circumference of the C_{60} molecule. The arrangement in Figure S4(e), with all $m = 4$ CF_3 radicals in para arrangement on adjacent hexagonal rings, is energetically the second-best isomer, with its energy only 0.051 eV higher than the most stable structure. The most stable isomer has a C_{2v} symmetry and the second most stable isomer only a mirror symmetry.

The structural paradigm for $La@C_{60}(CF_3)_m$ regioisomers with $m = 5$ CF_3 radicals is similar to the $m = 4$ case. Ten regioisomers are presented in Figure S5. The most stable of them, shown in Figure S5(a), contains 4 CF_3 radicals in para arrangement on three adjacent hexagonal rings. The last radical is separated by 4 neighbor distances from the closest CF_3 radical. It is also possible to arrange all five CF_3 radicals in para positions on four adjacent hexagonal rings. As seen in Figure S5(b), this highly symmetric regioisomer is less stable by $\lesssim$0.9 eV than the most stable structure.

References

1. Ganin, A. Y.; Takabayashi, Y.; Jeglič, P.; Arčon, D.; Potočnik, A.; Baker, P. J.; Ohishi, Y.; McDonald, M. T.; Tzirakis, M. D.; McLennan, A.; Darling, G. R.; Takata, M.; Rosseinsky, M. J.; Prassides, K. Polymorphism control of superconductivity and magnetism in Cs_3C_{60} close to the Mott transition. *Nature* **2010**, *466*, 221–225.

2. Nomura, Y.; Sakai, S.; Capone, M.; Arita, R. Unified understanding of superconductivity and Mott transition in alkali-doped fullerides from first principles. *Science Adv.* **2015**, *1*, e1500568.

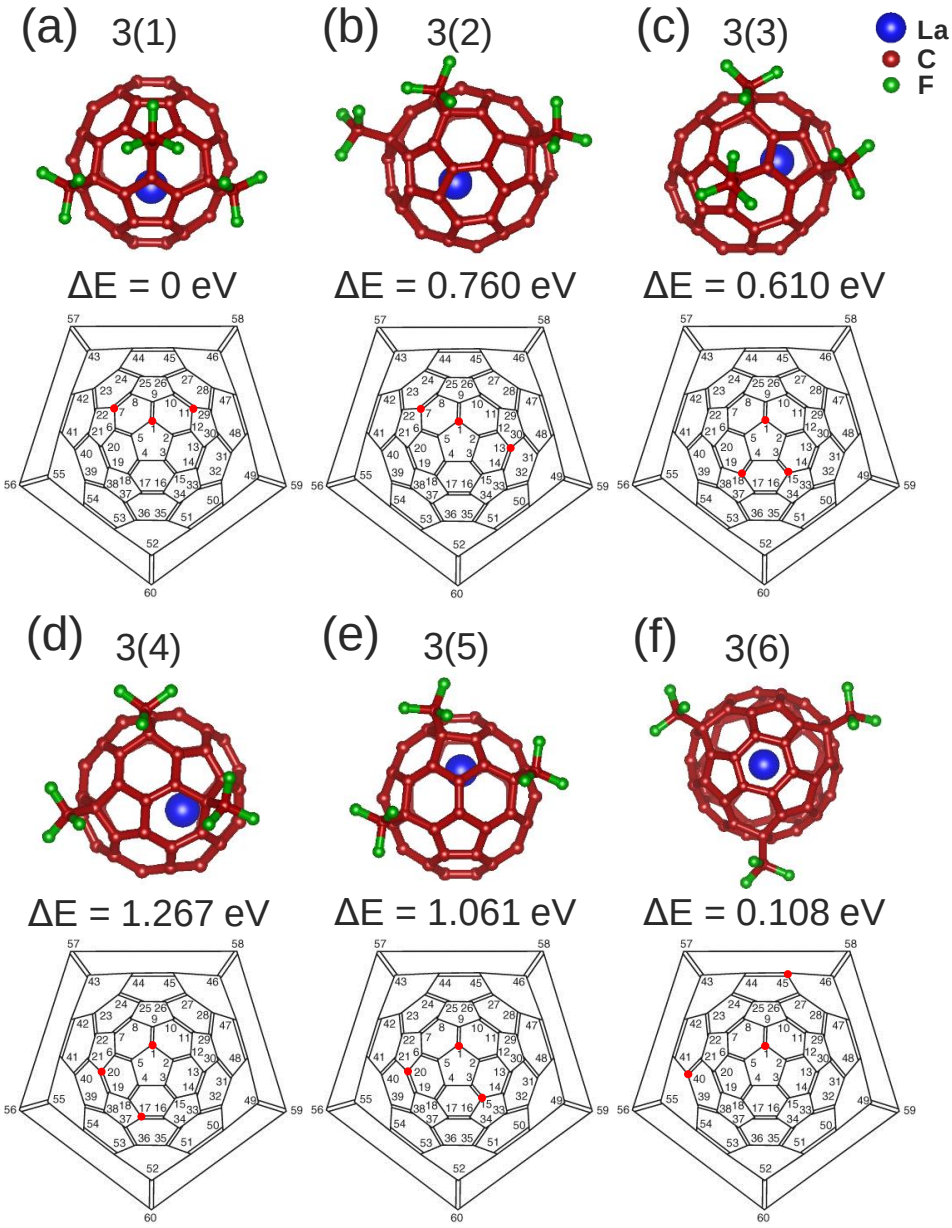

Figure S3: Six different La@$C_{60}(CF_3)_3$ isomers functionalized with 3 CF_3 radicals. The subfigures display the following isomers: (a) 3(1), (b) 3(2), (c) 3(3), (d) 3(4), (e) 3(5), (f) 3(6). The top panels show the ball-and-stick models of the structures, followed by the DFT-PBE relative total energy values ΔE with respect to the most stable isomer. The bottom panels show the Schlegel diagrams of functionalized C_{60} molecules, with the trifluoromethyl sites indicated by the red dots.

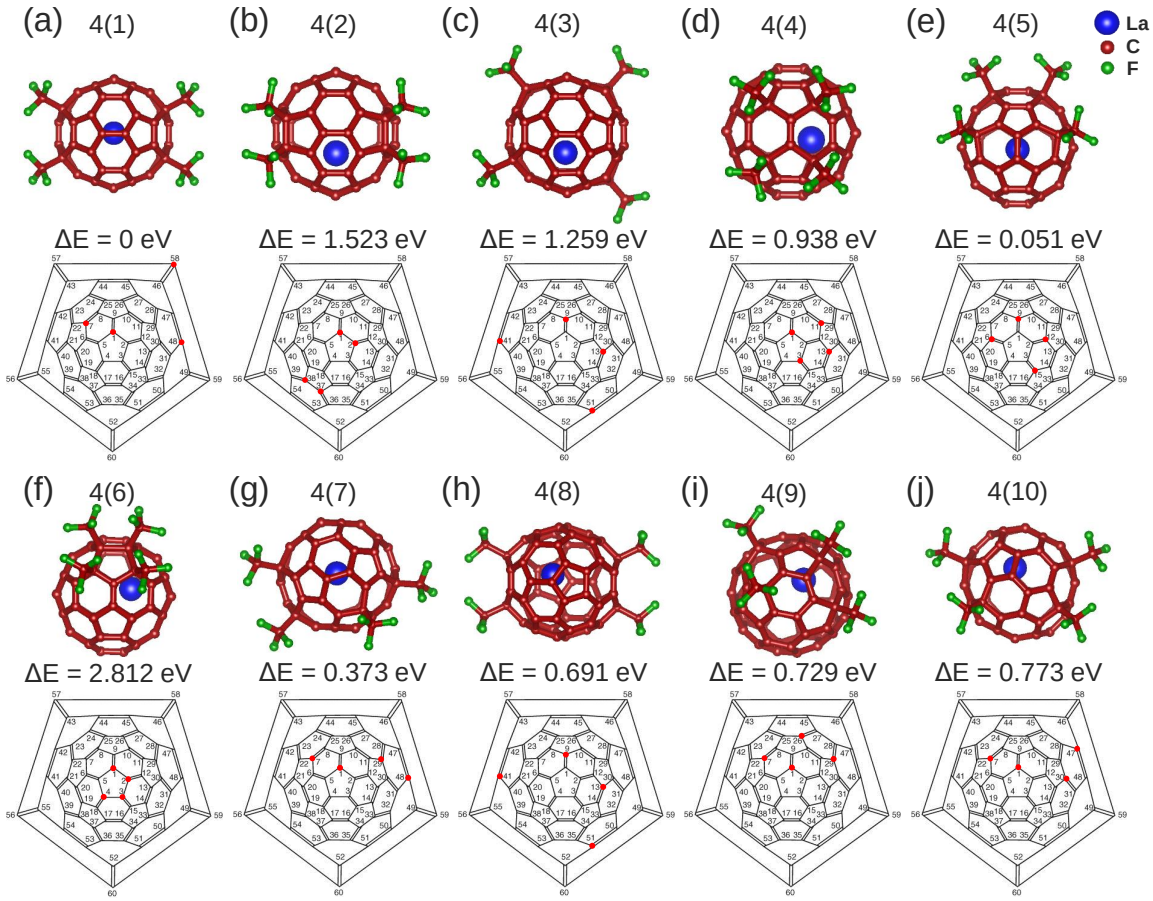

Figure S4: Ten different La@$C_{60}(CF_3)_4$ isomers functionalized with 4 CF_3 radicals. The subfigures display the following isomers: (a) 4(1), (b) 4(2), (c) 4(3), (d) 4(4), (e) 4(5), (f) 4(6), (g) 4(7), (h) 4(8), (i) 4(9), (j) 4(10). The top panels show the ball-and-stick models of the structures, followed by the DFT-PBE relative total energy values ΔE with respect to the most stable isomer. The bottom panels show the Schlegel diagrams of functionalized C_{60} molecules, with the trifluoromethyl sites indicated by the red dots.

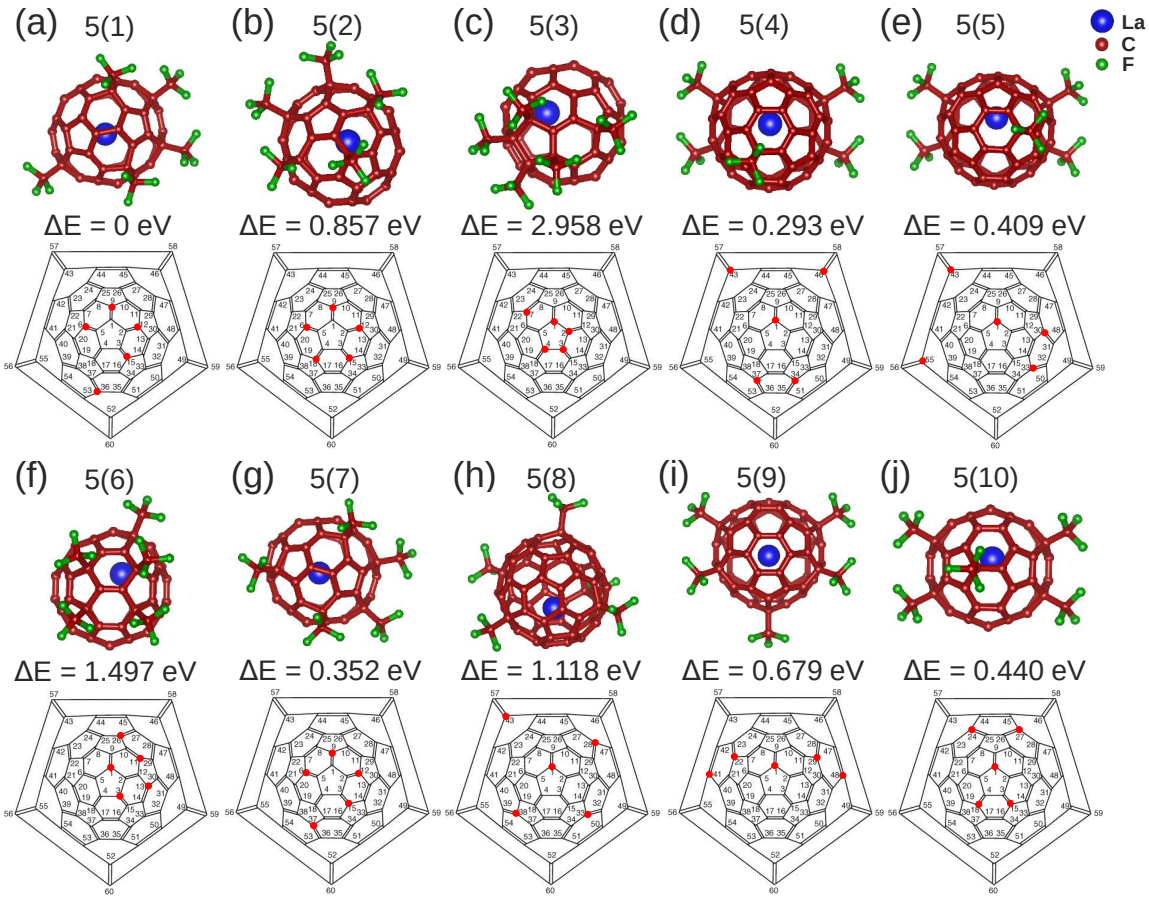

Figure S5: Ten different La@$C_{60}(CF_3)_5$ isomers functionalized with 5 CF_3 radicals. (a) 5(1), (b) 5(2), (c) 5(3), (d) 5(4), (e) 5(5), (f) 5(6), (g) 5(7), (h) 5(8), (i) 5(9), (j) 5(10). The top panels show the ball-and-stick models of the structures, followed by the DFT-PBE relative total energy values ΔE with respect to the most stable isomer. The bottom panels show the Schlegel diagrams of functionalized C_{60} molecules, with the trifluoromethyl sites indicated by the red dots.